UDC 550.83; 551.3; 551.794; 552.5: 523.681.8

Pavel KALENDA[1*], Lenka THINOVÁ[2], Rudolf TENGLER[3], Václav PROCHÁZKA[2], Jiří MIZERA[4], Petr MARTINEC[6], Günther KLETETSCHKA[5, 7], Tomáš TROJEK[2]

[1] CoalExp, Pražmo 129, 73904, Pražmo, Czechia, e-mail: pkalenda@volny.cz, https://orcid.org/0000-0003-4351-9593;
[2] Department of Dosimetry and Application of Ionizing Radiation, Faculty of Nuclear Science and Physical Engineering, Czech Technical University, 7, Břehová, 11519, Praha, 1, Czechia, e-mail: lenka.thinova@fjfi.cvut.cz, vaclav.prochazka@fjfi.cvut.cz, tomas.trojek@fjfi.cvut.cz, https://orcid.org/0000-0001-8277-1121, https://orcid.org/0000-0003-4320-7266, https://orcid.org/0000-0002-2136-4503;
[3] RTG-Tengler, 357/13, Českobratrská, 27601, Mělník, Czechia, e-mail: rtg@rtg-tengler.cz, https://orcid.org/0000-0002-0206-9605;
[4] Czech Academy of Sciences, Nuclear Physics Institute, 25068, Řež, Czechia, e-mail: mizera@ujf.cas.cz, https://orcid.org/0000-0002-8926-6213;
[5] Institute of Hydrogeology, Engineering Geology and Applied Geophysics, Faculty of Science, Charles University, Albertov 6, 12843, Praha 2, Czechia, e-mail: gunther.kletetschka@natur.cuni.cz, https://orcid.org/0000-0002-0645-9037;
[6] Czech Academy of Sciences, Institute of Geonics, Studentská, 1768, 708 00 Ostrava-Poruba, Czechia, e-mail: martinec@ugn.cas.cz, https://orcid.org/0009-0000-5084-6053;
[7] Geophysical Institute, University of Alaska – Fairbanks, 2156 N Koyukuk Drive, Fairbanks, AK 99775, USA.

https://doi.org/10.23939/jgd2024.02.027

TWO IMPACT CRATERS AT EMMERTING, GERMANY: FIELD DOCUMENTATION AND GEOPHYSICS

New research of two craters at Emmerting (No. 4 and No. 5), Germany, is presented. This paper should be the first part of two papers concerning presumed impact craters at Emmerting. The second paper will be about mineralogical / petrological, temperature and stress analyses. The enstatite-dominated meteoritic material, found in the crater No. 4 [Procházka et al., 2022; Procházka, 2023], is the subject of a separate detailed research. High-temperature effects and extreme deformation are significant in both craters. This deformation is explained with the effects of pressure wave(s) and later decompression in a target dominated by large but unconsolidated pebbles. Mutual collisions and secondary projectiles were documented. While most pebbles in the Crater No. 4 were thermally affected, the fine-grained fraction of the filling is poor in such material. It follows that small particles were volatilized and/or blown away during crater formation, or transported away later (e. g., by groundwater). Gamma-ray spectrometry has indicated that the walls of Crater No. 4 are significantly enriched in major natural radionuclides of Th, K and partly U, while the crater interior is depleted in these elements which are concentrated mainly in fine-grained fractions. This suggests a selective removal and volatilization of fine-grained material during the crater formation. The georadar measurements at both craters show that crater rims (walls) were partly pushed from below and partly heaped up from above with material that came from the crater interior. Georadar detected a compact body below the crater floor which is supported by results of resistivity measurements. A set of geophysical, geochemical, microscopic and mineralogical measurements proved that the craters at Emmerting are of impact origin. Extreme high temperature (HT) conditions inside the crater and small diameter of both craters indicate possible existence of very small meteoroids that are able to penetrate Earth´s atmosphere with high impact velocity (more than 30 km/s). This fact should challenge current models of bolide penetration through atmosphere.

Keywords: Holocene craters, terrace sediments, moraines, georadar, radiometric methods, automated resistivity system (ARES), cratering, impact craters.

Introduction

Looking for evidence of impact origin of small craters is challenging, unless the meteorite fall was observed and documented (e. g., [Plado et al., 2022] and references therein). As summarized in a recent review [Osinski et al., 2022], these craters usually form in the uppermost, less consolidated and porous rock material where the transformation of kinetic energy to shock waves, leading to shock metamorphism, is little efficient. The shock-metamorphosed material, if present at all, has small volume and is dispersed in relatively large space. Melting and high-temperature (HT) metamorphism is usually not an unequivocal proof of impact. In most small craters the impact origin was evidenced by finding of meteoritic iron. Out of all Holocene craters between 10 m and 200 m in diameter (i. e., not including the terminal pits), only in the Carancas crater (formed by a recent and witnessed impact) stone meteorite was found [Tancredi et al., 2009], see also [Osinski et al., 2022] and references therein).

The stone meteoroids entering the Earth's atmosphere with high velocity usually totally evaporate, or decay to small pieces and decelerate to such velocity, at which the dynamic pressure at the front of meteoroid is smaller than the tensile strength of the meteoroid (e. g., [Borovička, Kalenda, 2003]). Thus, it is not clear yet whether the impact of a relatively small stone

meteorite with velocity of several km/s is rather an exceptional event (in the case of Carancas facilitated by high altitude), or there are many such craters where, however, the stone meteorite relics decayed to such extent that they cannot be macroscopically identified (in humid climate hundreds of years are sufficient for that; see [Jull, 2001]).

On the other hand, hypervelocity cosmic collisions may be significant even in cases where the energy is totally, or prevalently, liberated in atmosphere (a classical example of such an explosion is the Tunguska event in 1908, and Chelyabinsk in 2013 [Kletetschka et al., 2017, 2015]). In-situ HT effects (up to vaporization), contamination with siderophile elements, unusual deformation, and probably also high-pressure effects, may occur even at sites where no impact crater was formed, as documented especially for the airburst at the base of Younger Dryas (e. g., [Moore et al., 2020; Bunch et al., 2021] and references therein). Thus, small hypervelocity impact craters may form as well.

In contrast to Northern Europe and the north-eastern Baltic region with many impact craters established, in Central Europe, only two hypervelocity impact events have been widely recognized up to now (according to the Earth Impact Database): the Miocene impact (possibly two separate impacts) which produced the Ries and Steinheim craters as well as the moldavite tektites, and the Morasko event in Holocene, forming several small craters. Recently, Berger (2014) summarized an unequivocal evidence for shock metamorphism in partly melted stones collected near Nalbach (Saarland, W. Germany); their geological position, however, is unclear, and the later announced "Nalbach crater" [Berger et al., 2015] has not yet been definitively accepted.

The small depressions at Emmerting and Grabenstätt-Kaltenbach (Bavaria, Germany) are located in the so-called Chiemgau Impact strewn field which, according to the proponents, contains more than 100 craters of Holocene age, formed most likely in the 1st millennium B. C., perhaps at the end of the Bronze Age [Rappenglück et al., 2004; Ernstson et al., 2010; Ernstson, 2017, Possekel and Ernstson, 2019]. The Chiemgau Impact strewn field would form an ellipse with small craters at NE and hypothetical large craters at SW. The lake Tüttensee was suggested to be the largest single crater (original diameter ca. 500 m [Rappenglück et al., 2004]), and a depression resembling a double crater with dimensions ca. 900×400 m at the bottom of the Chiemsee lake (Fig. 1) is the most prominent alleged impact structure [Ernstson, 2016] .

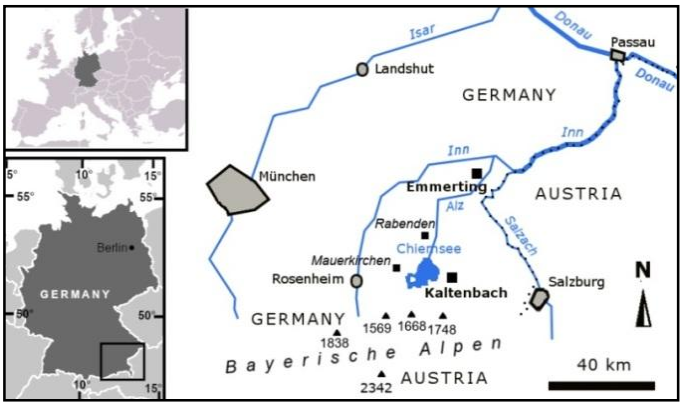

Fig. 1. Map of the region of interest showing the localities closely investigated (larger squares) and other localities briefly presented (small squares).
The impact origin of Tüttensee, however, has been questioned [Doppler, Geiss, 2005].

Detailed sedimentological research in the surroundings rather supports the original theory of a glacial kettle hole, and sedimentary profiles from the lake shore are rather undisturbed from the Late Glacial to recent (see [Huber et al., 2020; Rösch et al., 2021] and references therein). Also the impact into Chiemsee and subsequent tsunami were denied (see Huber et al., 2020 and references therein). Nevertheless, our paper has not been focused on discussion of the whole Chiemgau Impact hypothesis. We concentrate on the localities Emmerting and Kaltenbach where we collected samples, and HT-metamorphism and deformation have already been documented [Schüssler, 2005; Rösler et al., 2006; Neumair et al., 2016].

Purpose

Our aim is to document and explain the unusual combination of small dimensions of the craters with very intense thermal effects and deformation. This paper is concentrated mainly on field observation and geophysical measurements, and briefly summarizes macroscopic deformation and HT effects. Some results were presented at conferences [Procházka et al., 2021, 2022; Procházka, 2023].

Site description*Emmerting: Crater No. 4*

A walled crater with a diameter of the depression ca. 8 m and a diameter including walls up to 13 m (Fig. 2−4) is located ca. 1.5 km N of the center of the Emmerting town (48.21278°N, 12.7706°E, 410 m a. s. l) on a mild SE slope in a beech forest; the crater was cut by a trench for scientific purposes on the southern side.

Fig. 2. Crater No. 4 at Emmerting – intact position, view from W to E (photo: courtesy of W. Rösler).

Fig. 3. Crater No. 4 – the status in 2017 with a trench through the southern wall. View from S to N.

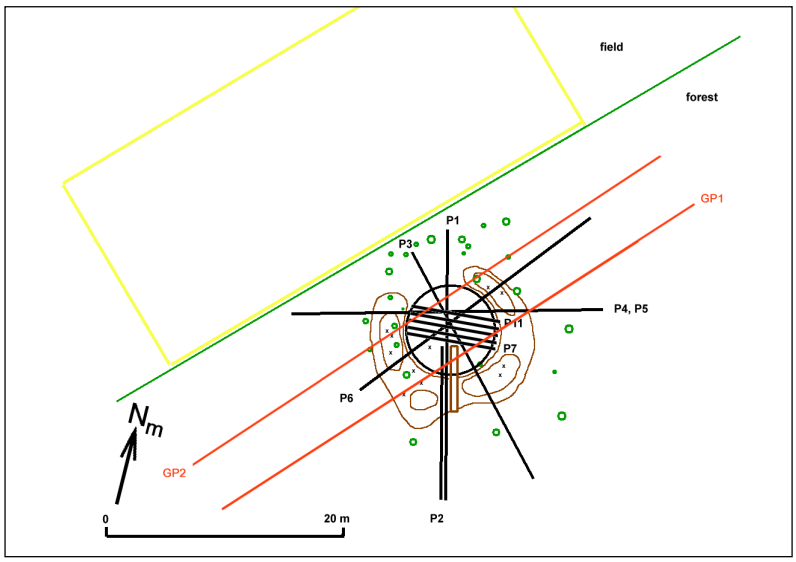

Fig. 4. The scheme of Crater No.004 at Emmerting and location of measured profiles (P1 to P11 were used for GPR, GP1 and GP2 for other geophysical methods). Green circles denote the trees; crosses denote the pebbles with glassy crust (at the crater's rim only).

The yellow rectangular area in the field was examined for glass-coated pebbles.e depression (crater) was formed in a Quaternary river terrace, containing typical pebbles transported from Alps, including sediments (prevalently limestone – carbonate rocks form about a half of pebbles in the area) as well as crystalline rocks. The terrace is the second one from the recent Alz river upwards (Niederterasse) whose age is Late Glacial [Anonymous, 1996]. Rösler et al. (2006) observed at least 100 years old trees growing from the wall as well as the crater interior. Various pebbles, frequently deformed, welded together with a silicate melt occur in the crater as well as in the wall, showing that the structure was heated as a whole and high temperature persisted for some time after its formation [Rösler et al., 2006]. Ernstson et al. (2010) suggested that another heat pulse happened, perhaps an explosion of methane from a cometary projectile.

Rösler et al. (2006) claimed lack of carbonate pebbles in the crater; similarly, only one out of 17 pebbles investigated by Schüssler (2005) was limestone. We collected enough limestone pebbles in 2015. Nevertheless, at the crater bottom as well as in the inner part of the wall (as documented in a trench), large amount of sharp-edged crushed limestone fragments can be found (similar to many small crater-like structures in the surroundings [Fehr et al., 2005]) which are sometimes sintered together. This can be explained partly by disintegration of relatively soft carbonate pebbles during crater formation, partly by decarbonization.

After georadar measurements in autumn 2015, we examined the field on the flat summit of the terrace as close as possible to the Crater No. 4 with the aim to find pebbles coated with glass (see Fig. 4). The field was clear and harrowed. The result was negative; in a rectangular area with dimensions 50×25 m, no glass-coated pebble was found. The same is true for material recently mined in the gravel pit at Emmerting.

Also geophysical contrasts were documented, especially by magnetometry [Rösler et al., 2006]. Several anomalies with magnetic susceptibility (MS) up to 0.0035 SI were found in the crater walls. The magnetic gradient measurement by the same authors showed monotonous surroundings of the crater but many dipole anomalies in the crater's wall. Most pebbles have high MS, often frequency dependent, which indicates presence of nanoparticles probably due to rapid temperature changes [Procházka, Kletetschka, 2016].

Ground penetrating radar (GPR) showed strong reflections from 2.7 to at least 7.5 m depth inside of the crater [Rösler et al., 2006], which has been attributed to "extreme sintering of the subsurface" [Possekel, Ernstson, 2019].

Extreme HT metamorphism, thermoplastic deformation and possibly volatilization were documented by Schüssler (2005) and Rösler et al. (2006). The melting was selective and little affected quartz even in rocks where eutectic melting of quartz should take place. Moreover, Schüssler (2005) and Rappenglück et al. (2010) presented extreme fracturing of mineral grains and indices for shock metamorphism (prevalently from petrographic microscope only): possible planar deformation features (PDF) of several directions in quartz and feldspar, diaplectic quartz, and spallation.

Fig. 5. Crater No. 5 at Emmerting before 2016. View from SE to NW (photo © PK 2015).

Other sites

Neumair and Ernstson (2011) mentioned rare glass coatings on rock fragments from the Mauerkirchen crater; we, however, haven´t found such material after digging to more than 0.5 m below the present bottom in the middle. The depression is partly filled with yellow clayey sediments which according to Neumair and Ernstson (2011) represent the bedrock, but they also could be a younger filling. At Rabenden, we found nothing unusual with possible exception of easily disintegrating pebbles of leucocratic orthogneiss, which are a rather exceptional phenomenon. It is questionable how they would have been able to survive transport from the Alps to Rabenden.

Emmerting: Crater No. 5

A walled crater with a diameter of the depression ca. 8 m, a diameter including walls up to 12 m and a depth of 1–1.2 m (Figs. 5, 6) is located ca. 2 km NNE of the center of the town Emmerting (48.2179°N, 12.7803°E, 390 m a. s. l) in a mixed forest. The target rocks are sediments (dominated by coarse pebbles) of the lowest terrace which is elevated ca. 3 m above the recent alluvium plane of the Alz river. The terrace age is Holocene [Anonymous, 1996]. The obviously thermally affected pebbles are rather less abundant than in Crater No. 4. Yellow sediment (marl?) could represent a younger autochthonous filling.

Grabenstätt – Kaltenbach

A walled circular depression with a 7–8 m diameter including walls is located at the summit of a forested moraine ridge near its eastern slope, 2 km east of the Chiemsee lake at the town Grabenstätt, west of the settlement Kaltenbach (47.8695° N, 12.5580° E, 575 m a.s.l.). Its filling contains mainly limestone cobbles (similar to the surroundings) commonly affected by decarbonization but also silicate cobbles and pebbles which were sometimes affected by melting. We checked and recognized more sites in the so-called Chiemgau crater field too, for example a crater at Mauerkirchen (47.89632° N, 12.32938° E) and a gravel pit at Rabenden (47.99437° N, 12.46182° E) where the georadar performance in typical coarse terrace sediments was tested (Appendix 1, Fig. A1).

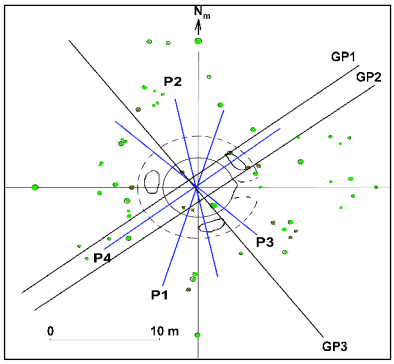

Fig. 6. The scheme of Crater No. 5 at Emmerting and location of measured profiles (P1 to P4 were used for GPR, GP1, GP2 and GP3 for other geophysical methods). Green circles denote the trees.

Methods

Ground penetrating radar (GPR, georadar)

A new kind of ground penetrating radar [Tengler, 2013] was employed, which uses pulses (sparks) instead of harmonic signals. This allows increasing the power output by at least three orders of magnitude in comparison with common GPRs. The 1-m long antenna was tuned to the central frequency of 150 MHz, which is comparable with previous measurement at Crater No. 4 [Rösler et al., 2006] but with the highly energetic impulses of 5 kV on antenna. This resulted in much deeper penetration depth, and the reflections from any reflecting plane or reflective body with permittivity contrast could be correctly registered from depths of at least 10 m (see Appendix 1, Fig. A1). Twenty pulses at the speed of the measurement about 1 km/h were summarized. The step between measurements was 0.1 m, GPS accuracy was better than 1 m. The length of each record was 1801 samples (crater No. 4) or 1081 samples (crater No. 5) and the step 0.277 ns (all together 500 ns / 300 ns). The sampling frequency was 3.6 GHz. Relative altitudes were measured by a barometer with the precision better than 10 cm.

Resistivity measurements (Automatic Resistivity System, ARES)

The ARES main unit with standard accessories and multi-electrode cable sections MCS5 was used. Six cable sections were used (8 copper electrodes at 1 m spacing each; 48 electrodes altogether) in Schlumberger and Dipole-Dipole arrays (both arrays were used for each measured profile). The distance between electrodes was 1 m. For the data interpretation a demo-version of the ARES SW was utilized. Three iterations only between measurement and modelled resulting data were used.

Magnetic susceptibility

Bulk susceptibility was determined with an SM-30 instrument (Z. H. Instruments, Brno). Exact measurement is possible for samples of 2×2×2 cm in size or larger. In addition, mass susceptibility at various field strengths (10–320 Am) and frequencies (502.6–7981 Hz) in small specimens from 7 pebbles was obtained at the Charles University, Prague, with the SM-100 apparatus (Z. H. Instruments, Brno).

Radon measurements

Radon activity was measured at 5 points of profile GP2 in Crater No. 4 using TESLA TSR 2 radon probes. The probe core consists of a measuring chamber with a semiconductor detector. Temperature and relative humidity are also measured. Measuring interval was set to 30 minutes. Because the probes are designated for indoor radon measurement, where the relative humidity does not exceed 70 %, a special geometry for radon measurement in soil was prepared. To protect probes from humidity and rain, each probe was covered with a plastic bag, and placed into a perforated Marinelli container (0.6 l). Such arrangement enabled that the soil gas flux coul reach the detector while a secure distance between the probe and bottom of the measurement hole was kept. The probes were inserted into a 35 cm depth (length of probe) and protected by a cover.

Field Gamma-Ray Spectrometry

In situ measurements of concentrations of K, U, Th and ^{137}Cs were performed mainly in the profiles. A portable GT40 spectrometer (Georadis, Brno) with a 3×3” NaI(Tl) detector was used. In addition, 10 points in the Kaltenbach structure and surroundings were measured with a GT30 instrument (^{137}Cs was not quantified). The sampling time was set to 3 minutes at each spot. The instruments are calibrated to 2π geometry and the depth range is usually 35–50 cm.

Results

Ground penetrating radar (GPR)

Crater No. 4

The results of the GPR measurement on all profiles confirmed the previous measurement [Rösler, 2006], but with better precision and resolution. We measured this site twice, in 2015 and in 2017. Because the measurements in 2017 only confirmed the results from 2015, only the results from 2015 have been analyzed. The filtered radarograms without topocorrections are presented in Fig. 7.

Fig. 8 shows the radarograms on the profile P1 with topocorrections according to barometer. The “column” radarogram, which supposed that the reflections are mostly coming vertically, is in Fig. 8, ***a*** and the radarogram, which supposed that reflections are mostly coming from the places perpendicular to the surface, is in Fig. 8, ***b***.

The deformations of the strata right below the crater can be seen on both radarograms in Fig. 8, independently on the method used. The greatest deformations are below the southern rim (right), where the wall is higher. The deformation is detectable to the depths of more than 20 m below the surface. The movement (with respect to the previous surface) should be more than 0.5−1 m, which corresponds with the depth of the crater (ca. 1 m). The same observation was mentioned by Rösler et al. (2006).

The most important body is the highly reflective layer(s) at a depth of 2–5 m right below the crater. This body consists of compact and hard breccia [Poßekel and Ernstson, 2019]); even drilling with a diamond drill was problematic (see also Appendix 1, Fig. A2). A compact, melt-cemented rock mass (perhaps representing the original crater’s floor) was also reached ca. 0.5 m below the present surface during the radon measurements. This body is a bit tilted to the north and is covered by soft sediment breccia at the crater bottom (Fig. 8).

To contour such a body, we made radarograms on profiles P7−P11 with the step 0.5 m. The radarograms without topocorrections are in Fig. 9. This body is practically below the whole bottom of the Crater No. 4. Its diameter is about 6 m and the thickness is 1−3 m.

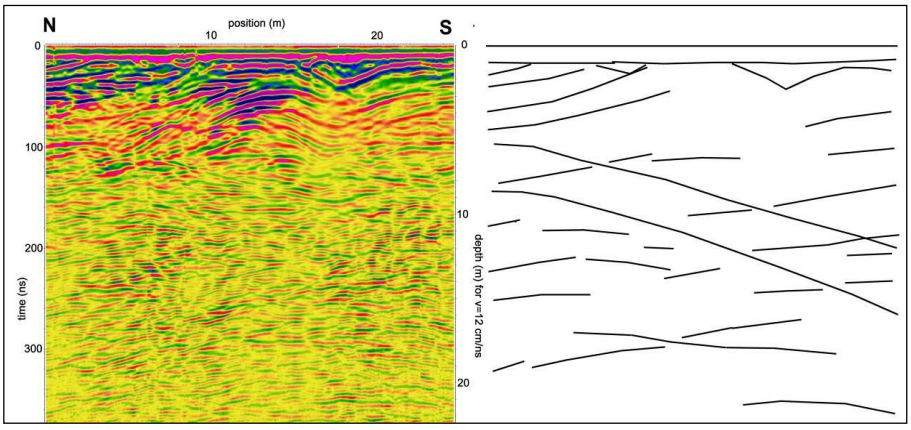

a

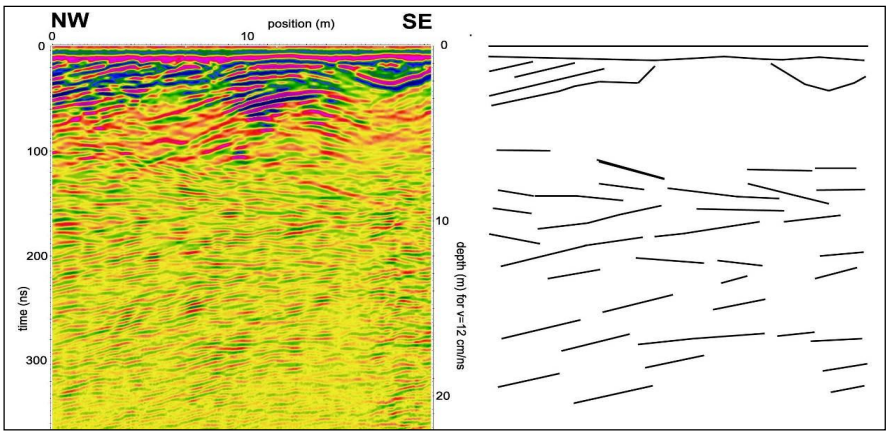

b

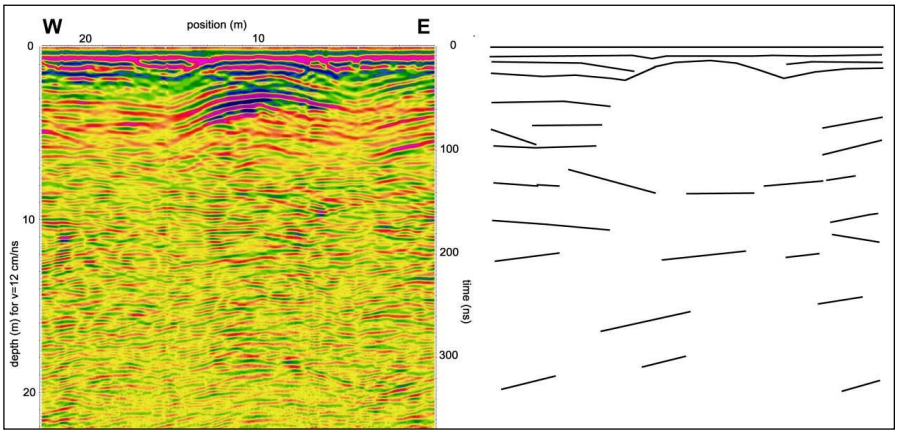

c

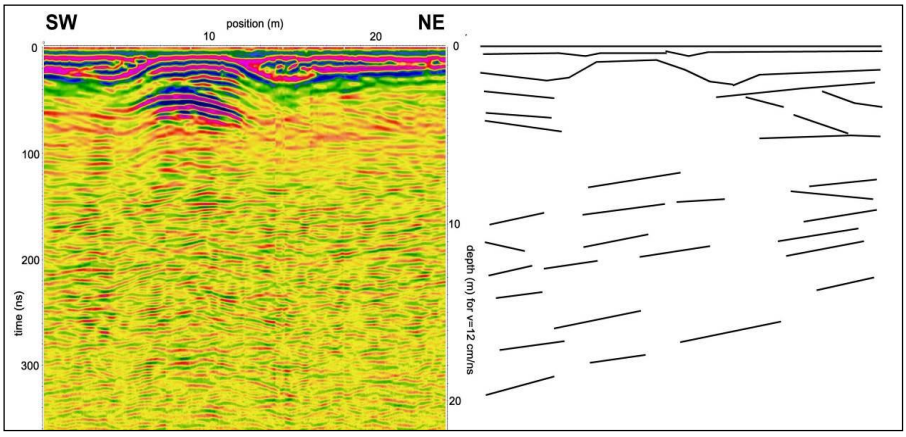

d

Fig. 7. Filtered radarograms without topocorrections and geological interpretation of the layers on the profiles P1 (a), P3 (b), P5 (c) and P6 (d), in the position “before impact”.

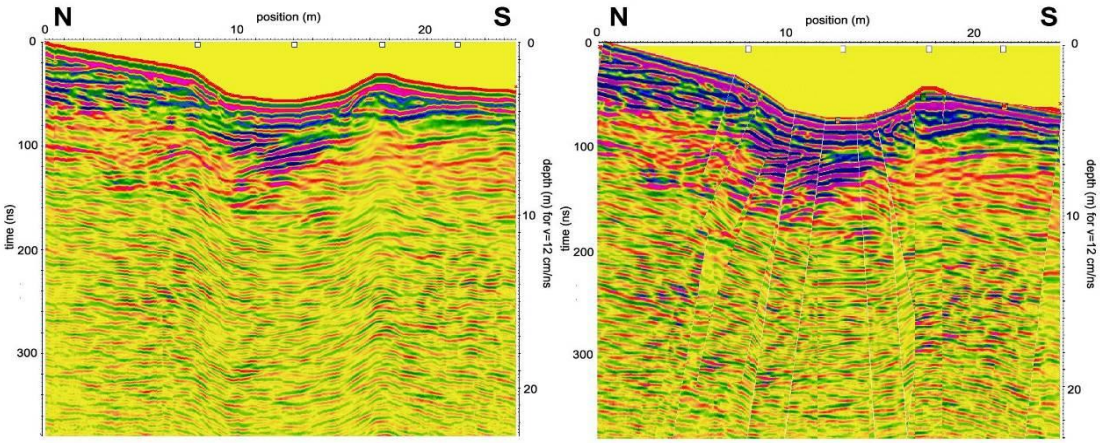

a b

Fig. 8. Filtered radarograms with topocorrections on the profile P1:
a – trace is vertical; b – trace is perpendicular to the surface (mosaic).

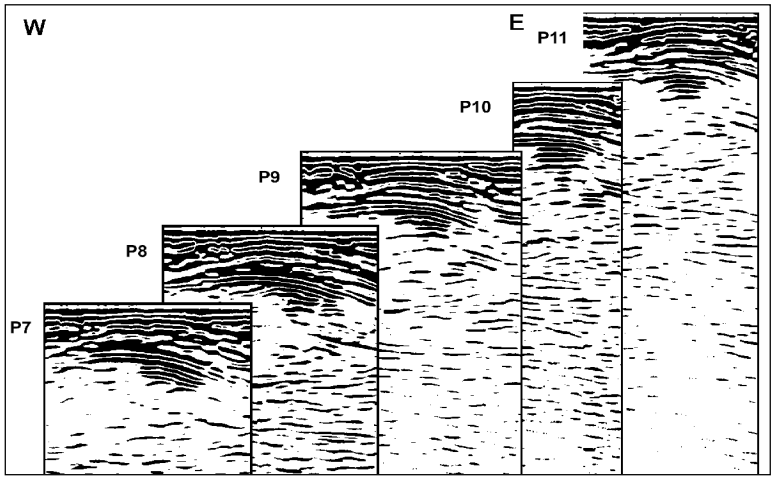

Fig. 9. Radarograms on profiles P7–P11 in the center of the Crater No. 4, pointing on the hard and compact body below the crater floor at a depth of 2–5 m.

Crater No. 5

We measured at this site in 2016. The filtered radarograms with topocorrections are presented in Fig. 10. A highly reflective body can be seen below the crater in the same way as in the Crater No. 4, even the depth is similar, 2–5 m below the crater floor. The crater rim is a bit different from the Crater No. 4, because a layer of soft sediments is thinner, and it seems that the material was only pushed up from the crater floor.

Resistivity measurements (ARES)

Crater No. 4

An area with lower resistivity was identified below the crater in both GP1 and GP2 profiles, with some asymmetry especially in GP2 (see Fig. 14).

The lower resistivity probably reflects higher water content. A possible interpretation, consistent with other methods, is the presence of a compact planar body below the crater, which is inclined to NE–NNE and somewhat retains the groundwater (note that such a body even in a small depth strongly influences signal from below).

The dipole-dipole measurement showed that the crater itself is filled by low resistivity sediments. Another potential small crater was localized at the end of profile GP2, in the distance approx. 20 m SW from the main crater (location −20 m).

Crater No. 5

The whole area was water-saturated during the measurement, which complicates the interpretation. The water in the bedrock is clearly visible on each resistivity cross section. The crater forms an obvious discontinuity in the ARES profiles, however, the results indicate some disturbance of its original shape (see Fig. 15). Presence of additional smaller craters is possible.

Gamma-ray spectrometry

The K, Th and U, and ^{137}Cs activities determined from the field gamma-ray spectrometry are presented in Appendix 1.

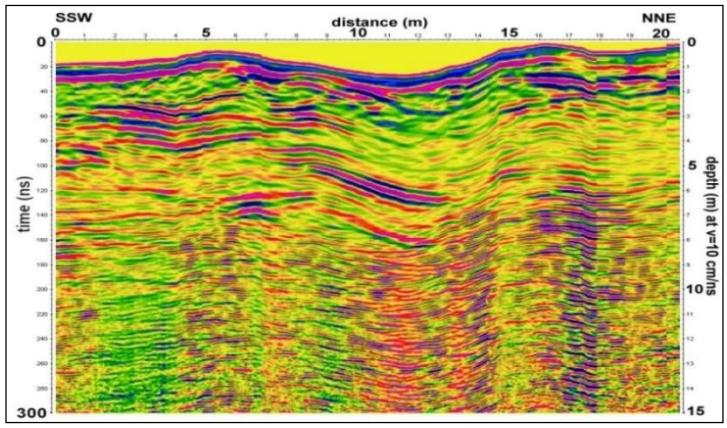

a

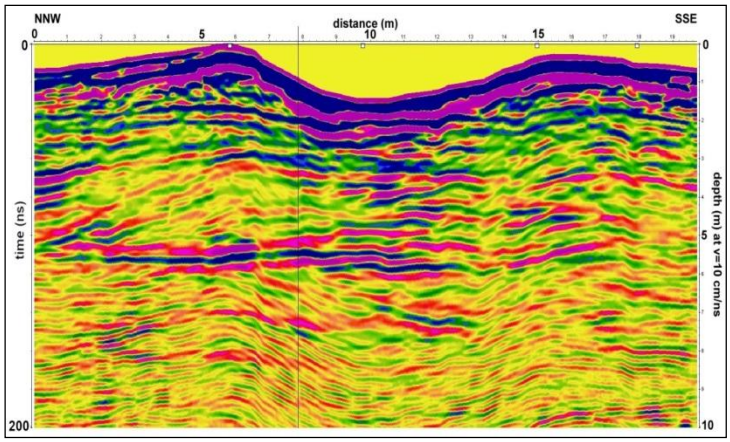

b

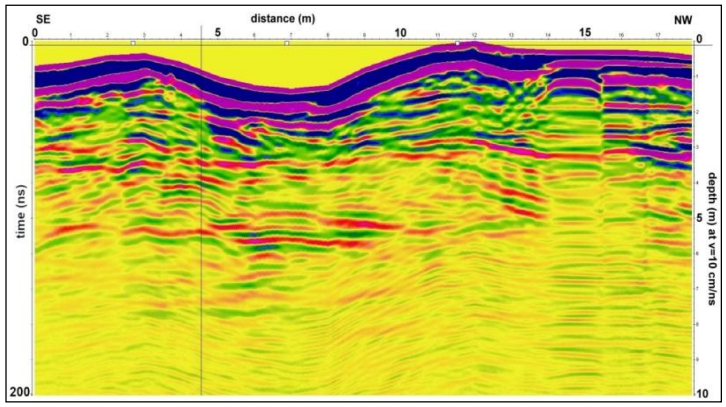

c

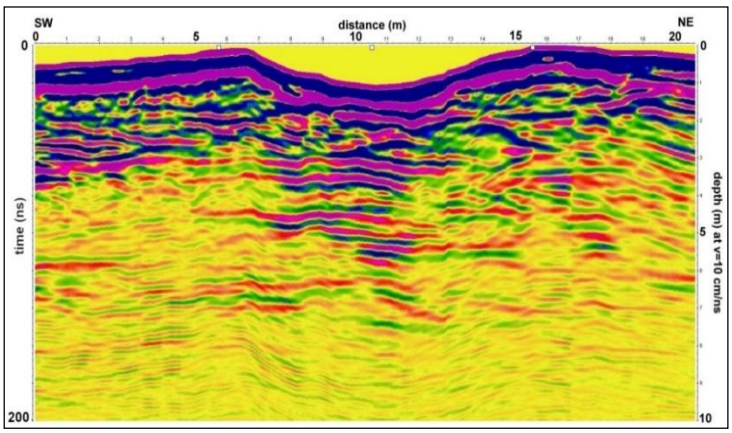

d

Fig. 10. Filtered radarograms with topocorrections on the profiles P1 to P4 (a−d), Crater No. 5.

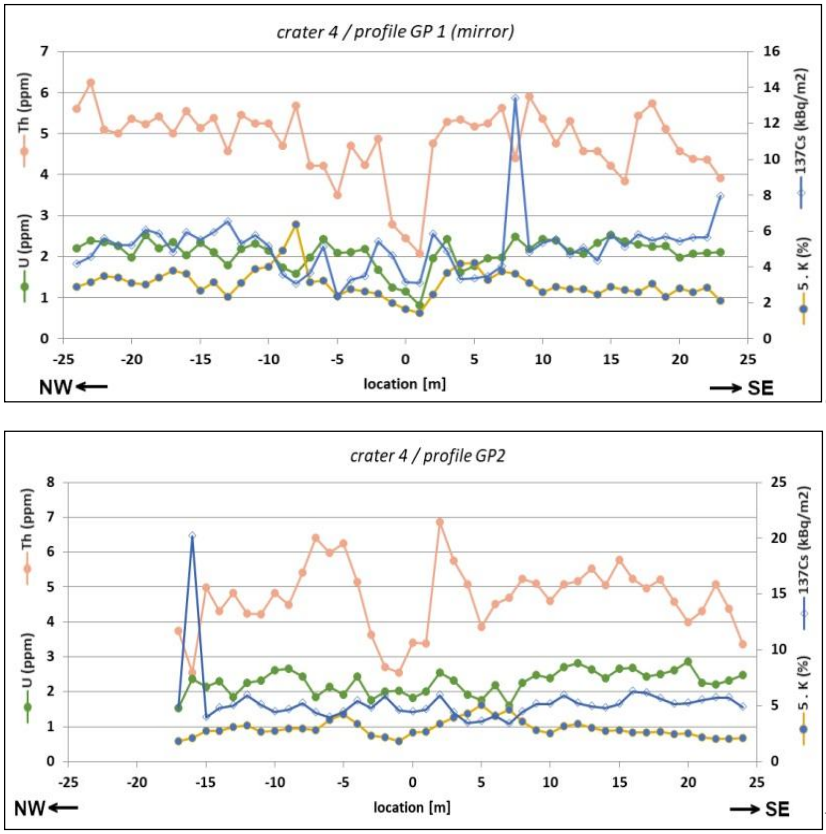

Fig. 11. Main radionuclides in two parallel profiles crossing the Crater No. 4 (zero is the crater center).

Compared to typical crustal values, concentrations of K, Th and U are very low, low, and low to average, respectively, reflecting composition of the pebbles which form the bedrock: high amount of limestone, calcareous sandstone and quartzite, low amount of granitic rocks and probable absence of alkaline igneous rocks (including their metamorphic equivalents), as well as low fraction of clay and silt in the terrace sediments. Thus, the K-rich glass coatings (Tab. 1) cannot be explained by influence of a hypothetic K-rich bedrock.

All radionuclides are depleted in the center of Crater No. 4 (Fig. 11). Importantly, this trend is most pronounced in the case of Th, a typical little mobile element. The depletion of the crater center in the anthropogenic ^{137}Cs which was deposited long time after crater formation is minor and is explainable by soil disturbance during research activities. On the other hand, K (and Th in the profile GP2) reaches peak values at the crater rim wall. In Crater No. 5 and its surroundings, the wet terrain and/or different petrography resulted in lower contents of the natural radionuclides measured. Considering the crater as a whole (not distinguishing the central depression and wall), it is somewhat enriched in K (see Fig. 12) and slightly depleted in ^{137}Cs, and perhaps slightly enriched in U and Th.

Two of four points measured in the Kaltenbach structure are significantly depleted in K and Th (including low Th/U ratios) in comparison with the relatively homogeneous surroundings of the crater (Appendix 1b).

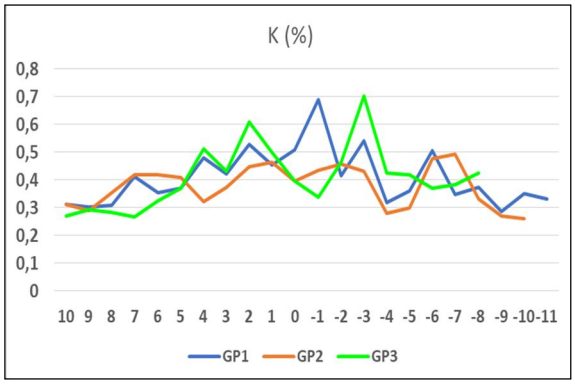

Fig. 12. Potassium weight concentrations in three profiles crossing the Crater No. 5.

Radon

(crater No. 4)

Radon activity varied from 2000 to 10000 Bq. m^{-3}. The maximal measurement error may be estimated according to the number of impulses recorded at about 10 %. The results could be interpreted in such way – consistent with GPR – that the bottom is formed by a plate of compact rocks, which is somewhat inclined to the northeast side of the profile. The relatively low

radon activity near the middle of the crater (especially at –3 m and –1 m, see Fig. 13) can be explained by a sealing effect of the plate. Lower Rn activity may also reflect lower U concentration in the crater filling.

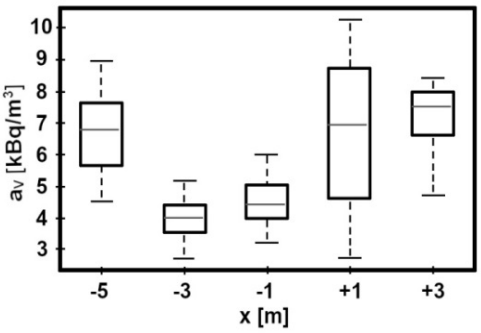

Fig. 13. Box-and-whisker plot of radon activity in soil gas (crater No. 4, profile GP2, SW–NE).

Summary and discussion of all field geophysical methods

Crater No. 4

The comparison of results of three methods in ca. SW-NE oriented profiles is presented in Fig. 14. All methods indicate a compact and watertight body below the crater floor.

In the GPR profile P6, the crater walls and compact body below the crater are well visible. The ARES measurement showed that the upper layers below the crater interior have low resistivity, which corresponds probably with the high content of mineralized water, which has been collected above the compact body. The western surroundings of the crater has higher resistivity than the eastern one, which can be interpreted as a consequence of the water flow from the crater to the northeast above the compact body below the crater interior.

Crater No. 5

In the GPR profile P4, the crater walls and a compact reflecting body below the crater are well visible. The situation inside the Crater No. 5 is very similar to the situation inside the Crater No. 4 from the GPR standpoint.

The ARES measurement have shown that the uppermost layers up to the depth of 0.5 m inside the crater and 1 m on the walls have partly relatively low resistivity. Within the 1–3 m depths, resistivity is relatively high. The crater interior and crater rim are not well visible in the dipole-dipole as well as in Schlumberger measurements. The low resistivity layers below the depth of 3 m correspond with water-filled sediments and probably with the groundwater level, which is at the depth of 3–5 m below the surface.

Magnetometry

Although specimens with high MS were not preferentially collected, it is obvious that MS is generally very high. In carbonates, however, it forms two distinct groups with values $<0.2\times10^{-3}$ SI and $>0.5\times10^{-3}$ SI, with maxima almost 1.5×10^{-3} SI (see Table 1 and Appendix 1, Table a)). All silicate pebbles and one of two vein quartz samples have mean MS$>0.25\times10^{-3}$ SI, and the peak value is 20.4×10^{-3} SI (relatively Fe-rich, hard and dense sandstone, Kaltenbach). Thus, the generally high MS of silicate rocks (as well as of some carbonates) is, very likely, related to the crater-forming event (see also [Ernstson et al., 2010]). However, anthropogenic origin of some angular stones at Kaltenbach cannot be excluded. Field dependence of MS was always positive in silicate rocks, but positive as well as negative field dependence occurs in limestones.

Discussion

The field observations and geophysical measurements are consistent with impact origin of the craters. Especially the compact body below the floor of Crater No. 4 (and possibly Crater No. 5 as well) is a strong indication for a highly unusual event. Such bodies may have formed by simple compression and reduction of pore spaces, but a role of melting and sintering, or of the formation of mortar-like matter thanks to decarbonization during the crater formation is also possible. Also note that hydration of reactive Ca-rich phases must have been an important heat source, and it would also efficiently remove liquid water. Moreover, possible relics of the reactive Ca-rich minerals would be strongly hygroscopic, which could explain low resistivity not only above but possibly also within the compact body.

The craters at Emmerting cannot be explained as glacial depressions (kettle holes) because during the last glacial period (Würmian in the classification for Alps), the glaciers have not reached the area of Emmerting. The closest young moraines of the Salzach Glacier from Alps [Van Husen, 1987] are located ca. 10 km to the south; moreover, the Crater No. 5 formed in a Holocene terrace [Anonymous, 1996]. Formation of perennial ice at the Kaltenbach site cannot be theoretically excluded, but it is highly improbable that it would form a small isolated circular depression near the top of a moraine ridge. Of course, any attempt to interpret the craters as glacial depressions should also explain the HT / HP effects (note that evidence for hypothetic human activities has not been found in the craters at Emmerting).

The impacts into targets dominated by large pebbles are little understood yet. Partly similar substrate rich in up to almost meter-sized coarse clasts (mainly of basalt) was documented in the Bajada del Diablo strewn field, but very few information about mineralogy, chemistry and deformation from these craters has been published [Acevedo et al., 2012]. Nevertheless, it can be expected that similarly to other porous environments, the temperature effects will be dominant [Kiefer, 1971; Osinski et al., 2022], while looking for classical shock effects like PDF in quartz can be little productive (see [Bunch et al., 2021]).

A probably non-impact nearly circular depression (the Tor structure, Sweden) has been recently investigated in a glacial till with boulders [Plado et al., 2022

Table 1

Overview of the first set of samples from Crater No. 4 (Emmerting) – basic characteristics, HT- and deformation processes, magnetic susceptibility

	Rock type	Crusts etc. (pre-impact)	In-situ fracturing	Glass coating, melting, traces of decarbonatization	Deformation during crater's formation and its relation to melting; secondary projectiles etc.	MS (10^{-3} SI)
1	quartzite with biotite *	partly bright crust	? (timing unclear)	thin colorless surface glass at one side	no	1.06–1.21
2	limestone	dark Mn oxides?	possibly very weak	surface decarbonization – white „chalk"	no	0.04–0.12
3	impure sandstone / quartzite? **	limonite in places?	widening fractures (rotation)	colorless glass coating + various contaminations (dark Fe-enriched melt)	extreme deformation with some pushing of external dark melt into wide fractures; limestone? stuck on the melt	1.72–7.11
4	quartzite with biotite *	limonite in places?	probably not	melting of biotite; colorless glass upside	expansion of biotite pulling apart the quartz grains	0.67–2.29
5	limestone	crust (corrosion layer)	possibly very weak	possibly decarbonization in places	no	0.45–0.99
6	dolomite	probably not	?	surface decarbonization – expanded layer	possibly irregular fracturing	0.32–0.88 **fr**
7	sandstone	minor Mn-oxides	not observed	joined by green glass with the diorite	no deformation inside observed	2.62–8.06
	diorite / granitoid?	not observed	probably in quartz	melting: feldspars and biotite	deformation after melting, including stretched bridges	
8	limestone	no	probable, irregular	locally surface decarbonization	no	0.07–0.09
9	sandy limestone *	silicate crust, limonite	possibly minor	thin glass (K-rich) covering silicate crust	no	0.16–0.45 **fr**
10	mica-schist or similar *	minor white crust	break-off	no	possibly some stretching (without melting)	0.11–0.74
11	vein quartz *	hollows after crystals	not observed	very thin glass cover in places	limited extension with stretched bridges	0.16–0.43
12	sandstone	locally lichen	probable	thin glass coating (except of bottom side)	no	0.62–0.72
13	sandy limestone?	corrosion	not significant	(?possibly decarbonization)	(?possibly expansion of CO_2)	0
14	vein quartz *	uncertain	? (break-off)	thin surface glass at one side	no	0
15	sandstone? **	limonite (in fracture), lichen	yes; break-off along older? fracture	colorless glass deposited from upside	open fractures after the strike, stretched bridges	2.39–7.54
16	orthogneiss?	locally limonite, carb.	probably in quartz	glass from feldspar and biotite	mainly gas expansion; secondary projectile (dark melt)	0.58–1.04
17	sandy limestone	corrosion layer, moss, leave fragments	possible (using calcite veinlets)	decarbonization of calcite veinlets, at least where they reached/formed the surface	only CO_2 expansion in original calcite	0.44–0.94 **fr**
18	quartzite with biotite	moss/lichen	probably not	„biotite" glass (mostly limonitized)	very limited expansion of biotite	7–11.3
19	basic rock (amphibolite?)	limonite	?	almost total melting (except of quartz? veinlets); greenish surface glass (K-rich)	strong expansion; surface contamination by limestone (also expanded)	0.32–0.79 fr
20	orthogneiss	weathering, lichen	not observed	colorless glass coating (K-rich); inside melting mainly of feldspars	(only microscopic expansion of gases)	0.65–2.01 fr
12	quartzite (impure)	limonite?	fractures in two directions filled with melt	melting of chloritized biotite and albite inside; surface colorless glass, younger black extrusions; „mixed" yellow, brown glass	probably widening of fractures (gas expansion); extrusions of black (mica-derived) melt; brown melt – influenced by surface contamination (Ca, Fe)	0.72–1.47 **fr**
22	quartz-albite rock (orthogneiss?)	weathering, lichen	open fractures, intense cleavage	no melting inside; thin colorless surface glass (K-rich)	extreme deformation with stretched bridges (locally mylonitization which may be older)	not measured

* significant part of the original pebble was broken off long time prior to sample collection (possibly even prior to crater formation)
** sample was neither cut nor broken in order to preserve the deformation figure undisturbed
fr – frequency dependence of MS was also measured (bold underlined in case that it is significant)

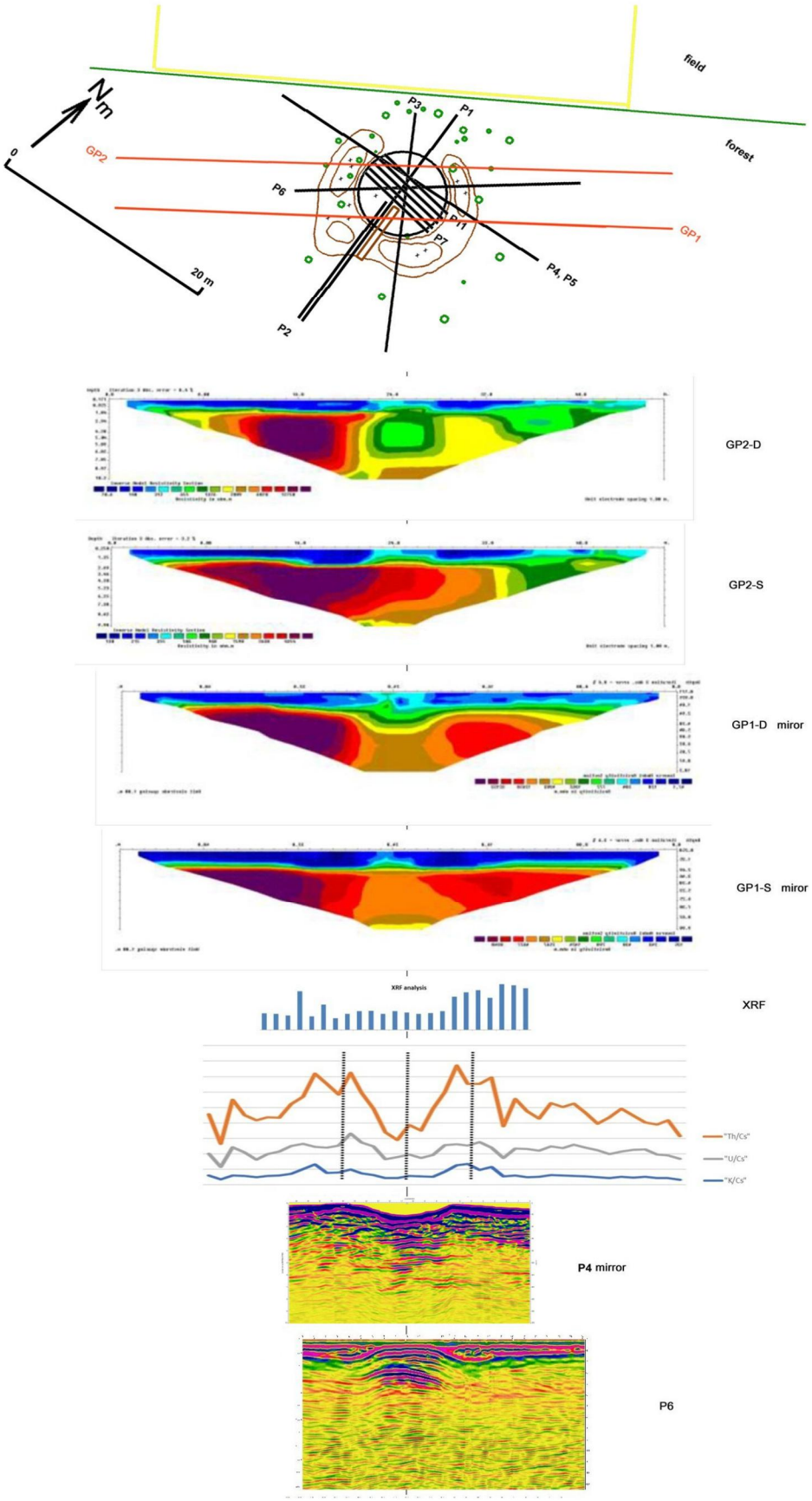

Fig. 14. Comparison of three geophysical methods:

ARES – dipole variant (D); ARES – Schlumberger variant (S), gamma spectrometry (mutual ratios of signals of Th, U and K to that of ^{137}Cs; mean from profiles GP1 and GP2), and GPR.

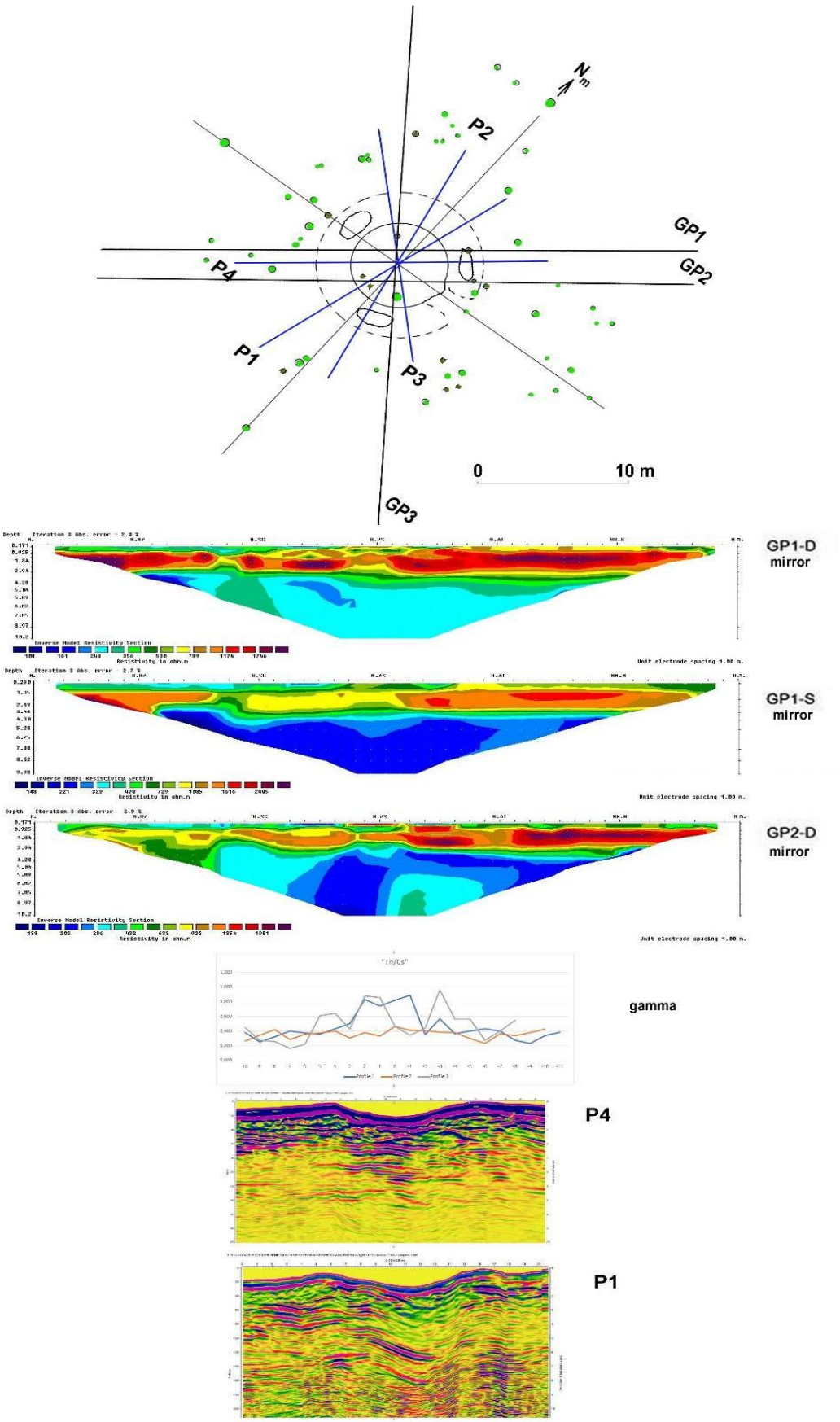

Fig. 15. Comparison of three geophysical methods:
ARES – dipole variant (D); ARES – Schlumberger variant (S),
gamma spectrometry (ratios of signals of Th and ^{137}Cs in three profiles), and GPR.

No HT-effects or unusual deformation have been observed in the Tor structure, the "crater" caused no anomaly in GPR profiles, and MS of its filling is not elevated [Plado et al., 2022].

Some specific features of crater formation in coarse but loose targets, perhaps reflecting additional heating and deformations caused by mutual collisions of pebbles after projectile explosion, were qualitatively documented by Procházka et al. (2021) and Procházka (2023). These effects include secondary projectiles, a phenomenon which perhaps has some analogy in literature [Anfinogenov et al. 2014].

Investigation of the meteoritic material found in the Crater No. 4 is ongoing. Its mineralogy and mineral chemistry [Procházka et al., 2022; Procházka, 2023] has some similarities with enstatite chondrites and aubrites but also important differences from representative composition of all meteorite groups known, possibly pointing to an unusual character of the impactor.

Originality and scientific novelty

A set of geophysical, measurements, consistent with results of other geological disciplines, proved that the craters at Emmerting are most probably of impact origin. These would thus be the smallest impact craters on Earth, where extremely high HT conditions were proven during their formation. Geophysical measurements showed that there is a compact body under the crater floor, created by strong compression, heating and melting of the sediments of this terrace.

Practical significance

Signs of extreme HT conditions found inside both studied craters with small diameters indicate that, under not quite understood conditions, even very small meteoroids should be able to penetrate Earth´s atmosphere, and survive while preserving a high impact velocity (more than 30 km/s). This fact should challenge current models of bolide penetration through atmosphere.

Conclusions

Impact origin of the Crater No. 4 has been supported by finding of a meteorite fragment, and observation of signs of the presence of a high temperature and uncommon strain effects. Similar features, although more rarely, have been observed in the crater No. 5 (Emmerting) and partly in the depression at Kaltenbach. We can speculate that a water-saturated environment (which is common here up to now) mitigated the strain and high temperatures in the Crater No. 5. Geophysical measurements at the craters No. 4 and 5 indicated potential compact features at and below their floors. These features were potentially formed by compression and/or thermal sintering and precipitation of Ca-rich minerals after HT-decarbonization.

The geophysical results have supported impact origin of the identified structures and completely rejected the anthropogenic hypotheses (limekilns) and postglacial phenomena.

Acknowledgements

The work was supported by the funding of the Ministry of Education, Youth and Sports of the Czech Republic, namely the project No. LM2023073 (Czech Technical Univ.), and the project for the long-term conceptual development of research organization RVO 68145535 (Institute of Geonics). We thank to Barbara and Michael Rappenglück, Hans-Peter Matheisl and Ernst A. Neugebauer for their help in the first sample collection campaign. Petra Vyletělová, Vojtěch Stránský and Tomáš Svoboda participated in some field measurements, and Kamila Johnová and Radek Prokeš in laboratory measurements. GK was partially supported by the Czech Science Foundation project, No. 23-06075S.

Appendix 1

a) mean concentration of radionuclides according to field gamma-ray spectrometry

	n	*K*, %	eTh, ppm	eU Ra, ppm	Th/U	^{137}Cs, kBq/m^2
ø C. 4 and surroundings	90	0.60	4.75	2.17	2.19	5.18
ø C. 5 and surroundings	62	0.50	2.50	1.50	1.67	5.84
ø C. Kaltenbach and surroundings	10	0.67	4.99	2.81	1.77	n. a.

b) comparison of concentrations of natural radionuclides according to field gamma-ray spectrometry in the Kaltenbach structure (individual measurements) and its surroundings (mean ± st. dev., *n*=6)

	K, %	eTh, ppm	eU Ra, ppm	Th/U
within the crater	0.69	5.4	2.9	1.86
	0.66	5.1	2.6	1.96
	0.31	3	2.4	1.25
	0.57	3	2.8	1.07
crater's surroundings	0.74 ± 0.11	5.6 ± 0.35	2.9 ± 0.28	1.93 ± 0.15

c) concentration of natural radionuclides in the soil (including small pebbles or their fragments; large biomass remnants were removed) determined by laboratory gamma-ray spectrometry

locality	*K*, %	Th, ppm	U (Ra parent), ppm	U, Ra daughter	^{137}Cs, Bq/kg
ø Crater 4 (*n*=4)	0.87	8.23	4.60	3.79	65
ø Crater 5 (*n* = 2)	0.515	5.75	3.4	2.67	69

d) approximate concentrations of natural radionuclides in individual silicate pebbles (laboratory gamma-ray spectrometry, samples not crushed; ^{137}Cs was below the limit of determination)

locality	rock type	sample No.	K, %	Th, ppm	eU Ra, ppm
Kaltenbach	sandstone	118	1.80	14.9	3.3
	orthogneiss	123	1.80	2.0	3.9
Emmerting 4	(meta)basic rock?	4/2/-1	1.25	1.4	0.5

Electronic Annex 1
The test of the ability of the georadar

Because of the serious concerns about possibilities of radar in the fluvioglacial sediments, we made a test of its ability in a similar locality. We have chosen the quarry south of Rabenden (47°59'45.09"N, 12°27'46.47"E), because the sequence of fluvioglacial sediments, similar to other sites investigated, is clear visible in the almost vertical walls there. We made one profile approximately 1 m parallel to the wall of the length of 33 m (see Fig. A1). The stones on the profile mark the position the same as was marked on the radarogram.

We can see the correctly detected strata on the radarogram and their inclination especially on the left part of the profile, where the inclination of several layers is higher than in the right part. Although we can verify the stratigraphy to the depth of only 5 m, the good quality reflections are visible from the depths to about 10 m.

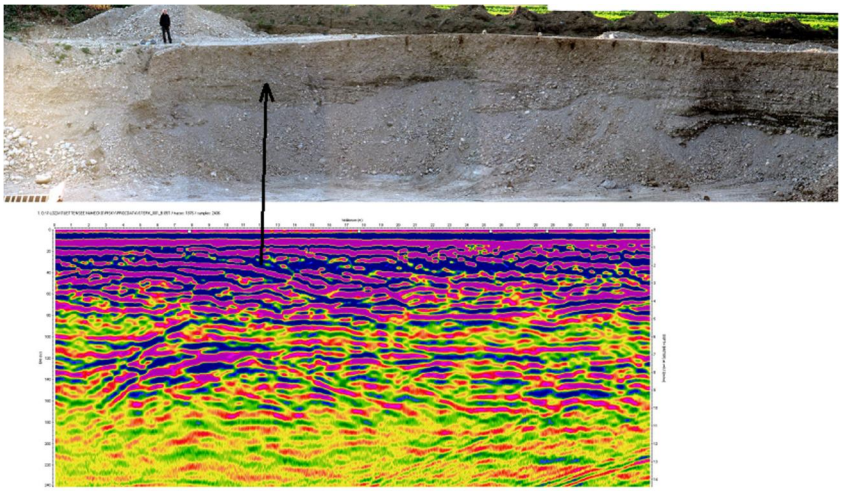

Fig. A1. The comparison of the real sedimentary profile and the radarogram.

Fig. A2. Shallow-drill core sample from the Crater No.004 at Emmerting, exhibited in the Chiemgau-Impact Museum, Grabenstätt, representing an unusually hard breccia.

References

Acevedo, R. D., J. Rabassa, J. F. Ponce, O. Martínez, M. J. Orgeira, C. Prezzi, H. Corbella, M. González-Guillot, M. Rocca, I. Subías, & C. Vásquez (2012). The Bajada del Diablo astrobleme-strewn field, central Patagonia, Argentina: Extending the exploration to surrounding areas. *Geomorphology*, 169−170, 151−164. https://doi.org/10.1016/ j.geomorph.2012.04.020

Anfinogenov, J., Budaeva, L., Kuznetsov, D., & Anfinogenova, Y. (2014). John's Stone: A possible fragment of the 1908 Tunguska meteorite. Icarus, 243, 139–147. https://doi.org/10.1016/j.icarus.2014.09.006.

Anonymous (1996). Geologische Karte von Bayern 1:500.000, 4. Auflage. Bayerisches Geologisches Landesamt, München (in German).

Berger, N. (2014). Analyse eines möglichen Meteoritenimpakts im Bereich der Prims (Nalbach, Saarland). Master thesis, Univ. Trier, 107 p. (in German).

Berger, N., Müller, W., & Ernstson, K. (2015). Strong shock metamorphism and a crater: evidence of a holocene meteorite impact event near Nalbach

(Saarland, Germany). In *46th Annual Lunar and Planetary Science Conference* (No. 1832, p. 1255).

Borovička, J., & Kalenda, P. (2003). The Morávka me¬teorite fall. 4. Meteoroid dynamics and fragmentation in the atmosphere. *Meteorit. & Planet.* Sci. 38(7), 1023−1043. https://doi.org/10.1111/j.1945-5100.2003.tb00296.x.

Bunch, T. E., M. A. LeCompte, A. V. Adedeji, J. H. Wittke, T. D. Burleigh, R. E. Hermes, C. Mooney, D. Batchelor, W. S. Wolbach, J. Kathan, G. Kletetschka, M. C. L. Patterson, E. C. Swindel, T. Witwer, G. A. Howard, S. Mitra, C. R. Moore, K. Langworthy, J. P. Kennett, A. West, & P. J. Silvia (2021). A Tunguska sized airburst destroyed Tall el Hammam a Middle Bronze Age city in the Jordan Valley near the Dead Sea. *Scientific reports*, 11(1), 1−64, https://doi.org/10.1038/s41598-021-97778-3.

Doppler, G., & Geiss, E. (2005). Der Tüttensee im Chiemgau–Toteiskessel statt Impaktkrater. Bayerisches Landesamt für Umwelt, online aufrufbar: https://www.lfu.bayern.de/geologie/meteorite/bayern/doc/tuettensee.pdf (letzter Zugriff: 10 (in German).

Earth Impact Database (accessed on August 21st, 2022). University of New Brunsvick, Canada.

Ernstson, K. (2016). Evidence of a meteorite impact-induced tsunami in Lake Chiemsee (Southeast Germany) strengthened. In *47th Annual Lunar and Planetary Science Conference* (No. 1903, p. 1263).

Ernstson, K. (2017). The Digital Terrain Model (DTM) and the evaluation of known and the search for new craters in the Chiemgau meteorite impact strewn field. Chiemgau Impact Research Team. URL: https://www.chiemgau-impakt.de/wp-content/uploads/2017/01/DGM-1-final-1.pdf.

Ernstson, K., Mayer, W., Neumair, A., Rappenglück, B., Rappenglück, M. A., Sudhaus, D., & Zeller, K. W. (2010). The Chiemgau crater strewn field: evidence of a Holocene large impact event in southeast Bavaria, Germany. *J. Sib. Federal Univ., Eng. Technol.*, 1, 72−103. https://cyberleninka.ru/article/n/the-chiemgau-crater-strewn-field-evidence-of-a-holocene-large-impact-event-in-southeast-bavaria-germany.

Fehr K. T., Pohl J., Mayer W., Hochleitner R., Faßbinder J., Geiß E., & Kerscher Y. (2005). A meteorite impact crater field in eastern Bavaria? A preliminary report. *Meteor. Planet.* Sci. 40, 187–194. https://doi.org/10.1111/j.1945-5100.2005.tb00374.x

Huber, R., Darga, R., & Lauterbach, H. (2020). Der späteiszeitliche Tüttensee-Komplex als Ergebnis der Abschmelzgeschichte am Ostrand des Chiemsee-Gletschers und sein Bezug zum. "Chiemgau Impakt" (Landkreis Traunstein, Oberbayern). *Quarternary Sci. J.* 69, 93−120 (in German). https://doi.org/10.5194/egqsj-69-93-2020.

Jull, A. J. T. (2001). Terrestrial ages of meteorites. In: Peucker-Ehrenbrink B., Schmitz B. (Eds.). Accretion of extraterrestrial matter throughout Earth's history. Springer US, Boston, 241–266. https://link.springer.com/chapter/10.1007/978-1-4419-8694-8_14.

Kiefer, S. W. (1971). Shock metamorphism of the Coconino Sandstone at Meteor Crater, Arizona. *J. Geophys. Res.* 76, 5449-5473. https://doi.org/10.1029/JB076i023p05449.

Kletetschka, G., Prochazka, V., Fantucci, R. & Trojek, T. (2017). Survival Response of Larix Sibirica to the Tunguska Explosion. *Tree-Ring Res.* 73, 75–90, https://doi.org/10.3959/1536-1098-73.2.75.

Kletetschka, G., Vyhnanek, J., Kawasumiova, D., Nabelek, L. & Petrucha, V. (2015). Localization of the Chelyabinsk Meteorite from Magnetic Field Survey and GPS Data. *Ieee Sensors Journal*, 15, 4875–4881, https://doi.org/10.1109/jsen.2015.2435252.

Moore, A. M., Kennett, J. P., Napier, W. M., Bunch, T. E., Weaver, J. C., LeCompte, M., ... & West, A. (2020). Evidence of cosmic impact at Abu Hureyra, Syria at the Younger Dryas onset (~12.8 ka): High-temperature melting at >2200°C. *Scientific Reports* 10, 4815, 22 p. https://doi.org/10.1038/s41598-020-60867-w.

Neumair, A., & Ernstson K. (2011). Geomagnetic and morphological signature of small crateriform structures in the Alpine Foreland, Southeast Germany. AGU Fall Meeting, No. GP11A-1023. https://ui.adsabs.harvard.edu/abs/2011AGUFMGP11A1023N/abstract

Neumair, A., Waitzinger, M., & Finger, F. (2016). Inte¬resting glass coatings on cobbles and rock fragments from the Alpine foreland, SE-Bavaria, Germany, and their possible origin. GeoTirol 2016, A233. https://uni-salzburg.elsevierpure.com/en/publications/interesting-glass-coatings-on-cobbles-and-rock-fragments-from-the.

Osinski, G. R., R. A. F. Grieve, L. Ferrière, A. Losiak, A. E. Pickersgill, A. J. Cavosie, S. M. Hibbard, P. J. A. Hill, J. J. Bermudez, C. L. Marion, J. D. Newman, & S. L. Simpson. (2022). Impact Earth: A review of the terrestrial impact record. *Earth-Sci. Rev.* 232, 104112, 48 p. https://doi.org/10.1016/ j.earscirev.2022. 104112).

Plado, J., Losiak, A., Jõeleht, A., Ormö, J., Alexanderson, H., Alwmark, C., Wild, E. M., Steier, P., Awdankiewicz, M., & Belcher, C. (2022). Discriminating between impact or nonimpact origin of small meteorite crater candidates: No evidence for an impact origin for the Tor crater, Sweden. *Meteor. Planet. Sci.*, 16 pp., https://doi.org/ 10.1111/-maps.13914.

Poßekel J., & Ernstson K. (2019). Anatomy of young meteorite craters in a soft target (Chiemgau impact strewn field, SE Germany) from ground penetrating radar (GPR) measurements. *50th LPSC*, A1204. https://ui.adsabs.harvard.edu/abs/2019LPI....50.1204P/abstract.

Procházka, V., & Kletetschka, G. (2016). Evidence for superaparamagnetic nanoparticles in limestones from Chiemgau crater field, SE Germany. *47th LPSC*, A2763. https://ui.adsabs.harvard.edu/abs/2016LPI....47.2763P/abstract.

Procházka, V. (2023). Melt behavior in two impact craters at Emmerting, Germany: Deformation,

expansion, injections, and the role of underpressure and mutual collisions of pebbles. *54th LPSC*, A2102.

Procházka V., Kalenda P., Trojek T., Faltus M. (2021): Geologicky mladé "zamrzlé" tavení hornin na několika lokalitách v Bavorsku: neobvyklý typ impaktu a výbuchy ve vzduchu? (Geologically young "frozen" melting of rocks at several sites in Bavaria: an unusual type of impact and explosions in the air?). *Proc. 26th Quaternary Seminary Meeting, Brno, Czech Republic.*

Procházka V., Martinec P., Štorc R., Kalenda P., Trojek T., Thinová L., Tengler R., Mizera J., (2022). Holocenní impaktní kráter u Emmertingu (Bavorsko): mineralogie výplně včetně meteoritu a možné vysvětlení kompaktního tělesa pode dnem kráteru (Holocene impact crater at Emmerting (Bavaria): mineralogy of the filling including meteorite and a possible explanation of the compact body below the crater bottom). *Proc. 27th Quaternary Seminary Meeting, Brno.*

Rappenglück M. A., Ernstson K., Mayer W., Beer R., Benske G., Siegl C., Sporn R., Bliemetsrieder T., & Schüssler U. (2004). The Chiemgau impact event in the Celtic Period: evidence of a crater strewnfield and a cometary impactor containing presolar matter. Chiemgau Impact Research Team. URL: https://www.chiemgau-impakt.de/pdfs/ Chiemgau_ impact.pdf.

Rappenglück B., Rappenglück M.A., Ernstson K., Mayer W., Neumair A., Sudhaus D., & Liritzis I. (2010): The fall of Phaethon: a Greco-Roman geomyth preserves the memory of a meteorite impact in Bavaria (southeast Germany). *Antiquity* 84, 428–439. https://doi.org/ 10.1017/S0003598X 00066680.

Rösch M., Friedmann A., Rieckhoff S., Stojako wits P., & Sudhaus D. (2021). A Late Würmian and Holocene pollen profile from Tüttensee, Upper Bavaria, as evidence of 15 Millennia of landscape history in the Chiemsee glacier region. *Acta Palaeobotanica*, 61/2, 136−147. https://doi.org/ 10.35535/acpa-2021-0008

Rösler W., Patzelt A., Hoffmann V., & Raeymaekers B. (2006). Characterization of a small crater-like structure in S.E. Bavaria, Germany. Proc. First International Conference on Impact Cratering in the Solar System, Noordwijk, pp. 67−71. European Space Agency.

Schüssler U. (2005). Chiemgau-Impakt: Petrographie und Geochemie von Geröllen mit Deformationsmerkmalen und starker thermischer Beanspruchung aus dem nördlichen Bereich des Impakt-Areals. Chiemgau Impact Research Team. (research report, 28 p.). URL: urn:nbn:de:101:1-201005228993.

Tancredi, G., Ishitsuka, J., Schultz, P. H., Harris, R. S., Brown, P., Revelle, D. O., Antier, K., Pichon, A. L., Rosales, D., Vidal, E., Varela, M. E., Sánchez, L., Benavente, S., Bojorquez, J., Cabezas, D. and Dalmau, A. (2009). A meteorite crater on Earth formed on September 15, 2007: The Carancas hypervelocity impact. *Meteor. Planet. Sci.*, 44: 1967−1984. ttps://doi.org/10.1111/j.1945-5100.2009.tb02006.x.

Tengler R. 2013. RTG-Tengler www pages. http:// georadar.rtg-tengler.cz/geologicky-zlom-u-sobotky.

Van Husen D. (1987). Die Ostalpen in den Eiszeiten. Veröffentlichung der Geologischen Bundesanstalt, 2, 24 p. (in German).

Павел КАЛЕНДА[1]*, Ленка ТІНОВА[2], Рудольф ТЕНГЛЕР[3], Вацлав ПРОХАЗКА[2], Їржі МІЗЕРА[4], Петр МАРТІНЕЦ[6], Гюнтер КЛЕТЕЧКА[5, 7], Томаш ТРОЙЕК[2]

[1] CoalExp, Пражмо, 129, 73904, Пражмо, Чехія, ел. пошта: pkalenda@volny.cz, https://orcid.org/0000-0003-4351-9593;

[2] Кафедра дозиметрії та застосування іонізуючого випромінювання, факультет ядерної науки та фізичної інженерії, Чеський технічний університет, Бржехова, 7, Прага 1, 11519, Чехія, ел. пошта: lenka.thinova@fjfi.cvut.cz, vaclav.prochazka@fjfi.cvut.cz, tomas.trojek@fjfi.cvut.cz, https://orcid.org/0000-0001-8277-1121, https://orcid.org/ 0000-0003-4320-7266, https://orcid.org/0000-0002-2136-4503;

[3] RTG-Tengler, Чеськобратрська, 357/13, Мельнік, 27601, Чехія, ел. пошта: rtg@rtg-tengler.cz, https://orcid.org/0000-0002-0206-9605;

[4] Чеська академія наук, Інститут ядерної фізики, Реж, 25068, Чехія, e-mail: mizera@ujf.cas.cz, https://orcid.org/0000-0002-8926-6213;

[5] Інститут гідрогеології, інженерної геології та прикладної геофізики, факультет природничих наук, Карлів університет, Альбертовб 6, Прага 2, 12843, Чехія, ел. пошта: gunther.kletetschka@natur.cuni.cz, https://orcid.org/0000-0002-0645-9037;

[6] Чеська академія наук, Інститут геоніки, Студентська, 1768, Острава-Поруба, 708 00, Чехія, ел. пошта: martinec@ugn.cas.cz, https://orcid.org/0009-0000-5084-6053;

[7] Геофізичний інститут, Університет Аляски – Фербенкс, 2156 N Коюкук Драйв, Фербенкс, Аляска 99775, США.

ДВА УДАРНІ КРАТЕРИ В ЕММЕРТІНГУ, НІМЕЧЧИНА: ПОЛЬОВІ ДОСЛІДЖЕННЯ ТА ГЕОФІЗИКА

Описано нові дослідження двох кратерів у Еммертінгу (№ 4 і № 5), Німеччина. Ця стаття – перша частина із двох статей, які стосуються ймовірних ударних кратерів у Еммертінгу. Друга стаття міститиме аналіз мінералогії / петрології, впливу температури та тиску. Метеоритний матеріал із домінуванням енстатиту, знайдений у кратері № 4 [Procházka et al., 2022; Procházka, 2023], – предмет окремого детального дослідження. В обох кратерах виявлено значні високотемпературні ефекти та екстремальні

деформації, які пояснюються впливом хвилі тиску та подальшої декомпресії в місці удару, де переважають великі, але рихлі гальки. Задокументовано взаємні зіткнення гальок та “вторинні снаряди” (викиди із кратера). Хоча більша частина гальки в кратері № 4 зазнала термічного впливу, дрібнозерниста фракція заповнення містить мало такого матеріалу. З цього випливає, що дрібні частинки випаровувалися та/або видувались під час утворення кратера, або переносилися пізніше (наприклад, ґрунтовими водами). Гамма-спектрометрія показала, що стінки кратера № 4 істотно збагачені основними природними радіонуклідами Th, K і частково U, тоді як внутрішній простір кратера збіднений ними, ці елементи зосереджені переважно в дрібнозернистих фракціях. Це свідчить про вибіркове видалення та випаровування дрібнозернистого матеріалу під час утворення кратера. Георадарні вимірювання в обох кратерах показали, що краї кратера (стінки) були частково витиснені знизу, а частково засипані зверху матеріалом, що надійшов із внутрішньої частини кратера. Георадар виявив компактне тіло під дном кратера, що підтверджують результати вимірювань питомого опору. Комплекс геофізичних, геохімічних, мікроскопічних і мінералогічних вимірювань довів, що походження кратерів у Еммертінгу ударне. Екстремально високі температури (НТ) всередині кратера та невеликий діаметр обох кратерів вказують на можливе існування дуже маленьких метеороїдів, які здатні проникати в атмосферу Землі із високою швидкістю удару (понад 30 км/с). Цей факт вважаємо викликом для моделей проникнення болідів через атмосферу.

Ключові слова: голоценові кратери, терасні відкладення, морени, георадар, радіометричні методи, автоматизована система вимірювання питомого опору (ARES), утворення кратерів, ударні кратери.

Received 2.02.2024